Perturbation Observer based Adaptive Passive Control for Damping Improvement of VSC-MTDC Systems

B. Yang[1,2], L. Jiang[2], Wei Yao[3,2], and Q. H. Wu[4,2]

Abstract

This paper proposes a perturbation observer based adaptive passive control (POAPC) for damping improvement of multi-terminal voltage source converter based high voltage direct current (VSC-MTDC) systems. The POAPC is designed for an N-terminal VSC-MTDC system, the perturbation is defined as a lumped term including interactions between terminals, unmodelled dynamics and unknown external disturbances, which is estimated online via a perturbation observer. Then an extra system damping is injected for each terminal to improve the transient dynamics via passivation. The POAPC does not require an accurate system model and measurements of full states, only the DC voltage, active and reactive power need to be measured. Case studies are carried out on a four-terminal VSC-MTDC system under four scenarios such as active and reactive power reversal, faults at AC bus, offshore wind farm connection, and fast time-varying parameter uncertainties. Simulation results verify its effectiveness under various operating conditions, compared with that of conventional proportional-integral (PI) control and classical passive control (PC).

Keywords

Adaptive passive control, perturbation observer, damping improvement, VSC-MTDC systems

Introduction

Voltage source converter based high voltage direct current (VSC-HVDC) systems based on insulated gate bipolar transistor (IGBT) switch have received numerous attentions in the last decade. The main feature of the VSC-HVDC system is that no external voltage source for commutation is required and the active and reactive power at each AC network can be independently controlled N. Flourentzou (2009). However, the traditional two-terminal VSC-HVDC system can only carry out point-to-point power transfer. As the economic development and the construction of power grids require the DC grid to achieve power exchanges among multiple power suppliers and multiple power consumers, multi-terminal VSC-HVDC (VSC-MTDC) systems attract many researches, which can easily achieve power exchanges among multipoints, connection between asynchronous networks, and integration of scattered power plants like offshore wind farms J. Liang (2011). For example, a VSC-MTDC system has been proposed for wind power transmission in Norway G. Asplund (2009) while the technology will be crucial for the European supergrid S. Gordon (2006). Recently, the world's first multi-terminal HVDC system employing VSC technology called Nanao's VSC-MTDC project has been built in China H. Rao (2015).

As the VSC-HVDC systems are highly nonlinear resulted from the converters and also operate in power systems with various system uncertainties, e.g. the ever-increasing penetration of renewable energy into the power system, it is very difficult to accurately model the power system equipped with VSC-HVDC systems. Thus, adaptive control systems design for the VSC-HVDC systems is needed to ensure a consistent control performance under various system uncertainties. Adaptive backstepping S. Ruan (2007) and multivariable optimal control G. Beccuti (2014) have been proposed to improve system dynamic performances which can estimate unknown constant or slow-varying system parameter. A robust sliding-mode control (SMC) was developed by A. Moharana (2010), which is insensitive to an assumed range of system parameter variations and external disturbances. Moreover, a singular value decomposition method is utilized to

[1]Faculty of Electric Power Engineering, Kunming University of Science and Technology, Kunming, 650504, China
[2]Department of Electrical Engineering and Electronics, University of Liverpool, Liverpool, L69 3GJ, United Kingdom
[3]State Key Laboratory of Advanced Electromagnetic Engineering and Technology, Huazhong University of Science and Technology, Wuhan, 430074, China
[4]School of Electric Power Engineering, South China University of Technology, Guangzhou, 510641, China

Corresponding author:
L. Jiang, Department of Electrical Engineering and Electronics, University of Liverpool, Liverpool, L69 3GJ, United Kingdom
Email: ljiang@liverpool.ac.uk

select the most effective damping control signal of the VSC-HVDC output feedback controllers with a fuzzy logic based power system stabilizer (PSS) P. Farhang (2014).

However, the above applications are limited to two-terminal VSC-HVDC systems. Several adaptive control schemes have been developed for VSC-MTDC systems, such as adaptive droop control N. Chaudhuri (2013), which can share the burden according to the available headroom of each converter station. An adaptive backstepping droop controller is proposed in X. Zhao (2015), which can adaptively tune the droop gains to enhance control performances of traditional droop controllers by considering DC cable dynamics. Based on probabilistic collocation method, the modal linear quadratic Gaussian controller structure was tuned for a set of probabilistic values of critical eigenvalues to improve the system damping in R. Preece (2014). In order to improve the proportional-integral (PI) control performance, fuzzy logic-based PI controllers have been designed by K. Meah (2008, 2010), which can provide an optimal operating range to handle system uncertainties and nonlinearities of VSC-MTDC systems by auto-tuning the PI gains. However, the tuning burden will be significantly increased when the number of terminals grows as four interacted PI gains need to be simultaneously tuned in each terminal.

In the past decades, several elegant approaches based on observers have been proposed to estimate system uncertainties, including the unknown input observer (UIO) C. Johnson (1971), disturbance observer (DOB) W. Chen (2000), perturbation compensator based on sliding-mode observer S. Kwon (2004), uncertainty and disturbance estimator (UDE) Q. Zhong (2004), nonlinear observer based active disturbance rejection control (ADRC) J. Han (2009), ect. Moreover, a systematic and comprehensive tutorial and summary on the existing disturbance/uncertainty estimation and attenuation techniques have been investigated in S. Li (2014), such as disturbance accommodation control (DAC), composite hierarchical anti-disturbance control (CHADC), and generalized proportional integral observer (GPIO), ect. W. Chen (2016). In general, these observers can provide great robustness to external disturbances or unmodelled dynamics. Among the above listed approaches, extended state observer (ESO) based approaches S. Kwon (2004); J. Han (2009) require the least amount of system information. Thus, perturbation observer based adaptive passive control (POAPC) scheme developed by the author B. Yang (2015) is employed for an N-terminal VSC-MTDC system, in which the combinatorial effect of interaction between terminals, unmodelled dynamics and unknown time-varying external disturbances is aggregated into a perturbation term, which is estimated online by an ESO called high-gain state and perturbation observer (HGSPO) Q. Wu (2004); J. Chen (2014); B. Yang (2015). POAPC does not require an accurate system model and only the DC voltage, active and reactive power need to be measured. Once it is set up for the VSC-MTDC system within a predetermined range of variation in system variables, no tuning is needed for start-up or compensation of changes in the system dynamics and disturbance. Moreover, the proposed controller can improve the system damping via passivation D. Flores (2014); L. Harnefors (2015), hence it is able to reduce the overshoot of active and reactive powers for different operating conditions.

The contribution and novelty of this paper compared to our previous work Q. Wu (2004); J. Chen (2014); B. Yang (2015) can be summarized as follows:
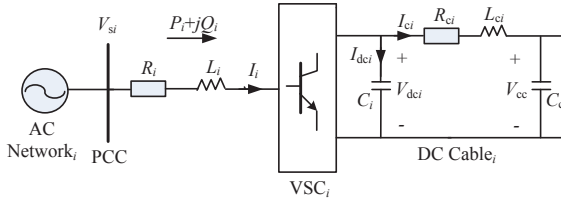
Figure 1. One terminal of an N-terminal VSC-MTDC system.

• Compared to Q. Wu (2004); J. Chen (2014) which only deal with the system uncertainties by perturbation estimation, this paper exploits the system physical property via passivation to improve the system damping, such that a better system transient response to system faults can be achieved;

• Compared to B. Yang (2015) which requires one subsystem's relative degree must be one and accurate information of some system variables or parameters, this paper does not need such requirements thus it can be applied on more practical applications.

The control performance of the POAPC is evaluated on a four-terminal VSC-MTDC system, in which the tracking performance of active and reactive power is evaluated at first. Then the enhancement of system transient responses is discussed under the AC bus fault and offshore wind farm connection, respectively. Finally, the system robustness is tested in the presence of parameter uncertainties. Simulation results are provided to demonstrate its superiority over that of PI control and passive control (PC).

VSC-MTDC System Modelling

The mathematical model of an N-terminal VSC-MTDC system is established in the synchronous *dq* frame. A lumped parameter model is assumed and the AC network is represented through the series connection of the AC network voltage source and transmission line, which is interfaced to a VSC at the point of common coupling (PCC). A more detailed VSC model featuring the related switches can be employed but this would only add a slight ripple in voltage waveforms due to the associated switch action, which does not significantly affect the fundamental dynamics G. Beccuti (2014), thus VSCs are represented by the average model N. Chaudhuri (2013).

The *dq* frame is placed on AC terminals, during the transformation of the *abc* frame to the *dq* frame, the D-Q-Z-type phase-locked loop (PLL) is used due to its excellent interharmonic cancellation and transient response D. Jovcic (2003). The d-axis is locked with the voltage V_{si} on the ith AC terminal of VSCs to ensure a decoupled control of the active and reactive power. Only the balanced condition is considered in this paper, i.e., the three phases have identical parameters and their voltages and currents have the same amplitude while each phase shifts $120°$ between themselves.

One terminal of an N-terminal VSC-MTDC system is illustrated in Fig. 1. On the ith AC terminal of the VSC, the system dynamics can be expressed at the angular frequency

ω_i as N. Chaudhuri (2013)

$$\begin{cases} \dot{I}_{di} = -\frac{R_i}{L_i}I_{di} + \omega_i I_{qi} + \frac{V_{sqi}}{L_i} + \frac{u_{di}}{L_i} \\ \dot{I}_{qi} = -\frac{R_i}{L_i}I_{qi} + \omega_i I_{di} + \frac{V_{sdi}}{L_i} + \frac{u_{qi}}{L_i} \end{cases} \tag{1}$$

where I_{di} and I_{qi} are the ith d-axis and q-axis AC currents; V_{sdi} and V_{sqi} are the ith d-axis and q-axis AC voltages, in the synchronous frame $V_{sdi} = 0$ and $V_{sqi} = V_s$; u_{di} and u_{qi} are the ith d-axis and q-axis control inputs; and R_i and L_i are the aggregated resistance and inductance of the ith AC terminal, respectively.

By neglecting the resistance of VSC reactors and switch losses, the instantaneous active power P_i and reactive power Q_i on the ith AC terminal can be calculated as follows

$$\begin{cases} P_i = \frac{3}{2}(V_{sqi}I_{qi} + V_{sdi}I_{di}) = \frac{3}{2}V_{sqi}I_{qi} \\ Q_i = \frac{3}{2}(V_{sqi}I_{di} - V_{sdi}I_{qi}) = \frac{3}{2}V_{sqi}I_{di} \end{cases} \tag{2}$$

The DC link dynamics can be expressed by

$$\begin{cases} \dot{V}_{dci} = \frac{1}{V_{dci}C_i}P_i - \frac{1}{C_i}I_{ci} \\ \dot{I}_{ci} = \frac{1}{L_{ci}}V_{dci} - \frac{R_{ci}}{L_{ci}}I_{ci} - \frac{1}{L_{ci}}V_{cc} \end{cases} \tag{3}$$

The topology of an N-terminal VSC-MTDC system is illustrated by Fig. 2, in which the dynamics of the common DC capacitor can be obtained according to the Kirchhoff's current law as K. Meah (2008)

$$\dot{V}_{cc} = \frac{1}{C_c}\sum_{i=1}^{N}I_{ci} \tag{4}$$

where C_i and C_c are the ith DC link capacitance and the common DC capacitance which voltages are denoted by V_{dci} and V_{cc}; R_{ci} and L_{ci} are the resistance and inductance of the ith DC cable; and I_{ci} is the current through the ith DC cable. The featured DC cable model corresponds to a simplified equivalent of a cable connection, because an overhead line could be represented by an inductive element N. Flourentzou (2009). This is a reasonable approximation for the purpose of control systems analysis.

To this end, the global model of the N-terminal VSC-MTDC system can be written as follows

$$\begin{cases} \dot{I}_{di} = -\frac{R_i}{L_i}I_{di} + \omega_i I_{qi} + \frac{V_{sqi}}{L_i} + \frac{u_{di}}{L_i} \\ \dot{I}_{qi} = -\frac{R_i}{L_i}I_{qi} + \omega_i I_{di} + \frac{u_{qi}}{L_i} \\ \dot{V}_{dci} = \frac{3V_{sqi}I_{qi}}{2V_{dci}C_i} - \frac{1}{C_i}I_{ci} \qquad\qquad , i = 1,\ldots,N \\ \dot{I}_{ci} = \frac{1}{L_{ci}}V_{dci} - \frac{R_{ci}}{L_{ci}}I_{ci} - \frac{1}{L_{ci}}V_{cc} \\ \dot{V}_{cc} = \frac{1}{C_c}\sum_{i=1}^{N}I_{ci} \end{cases} \tag{5}$$

Perturbation Observer based Adaptive Passive Control

Consider a single-input single-output (SISO) system as

$$\begin{cases} \dot{x} = Ax + B(a(x) + b(x)u + \xi(t)) \\ y = x_n \end{cases} \tag{6}$$
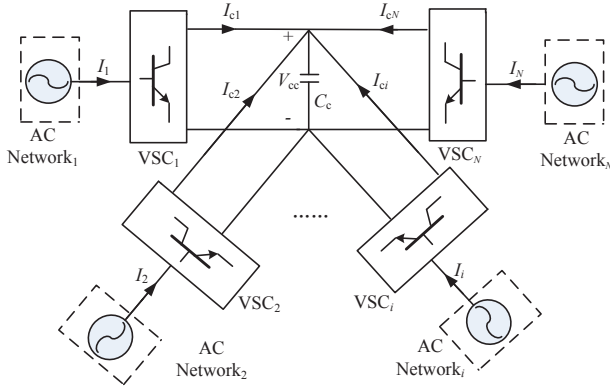
Figure 2. The topology of an N-terminal VSC-MTDC system.

where $y \in \mathbb{R}$ is the output and $u \in \mathbb{R}$ is the input; $\mathbf{x} = [x_1, x_2, \cdots, x_n]^{\mathrm{T}} \in \mathbb{R}^n$ is the state vector; $a(x) : \mathbb{R}^n \mapsto \mathbb{R}$ and $b(x) : \mathbb{R}^n \mapsto \mathbb{R}$ are C^∞ unknown smooth functions; $\xi(t) \in \mathbb{R}$ is the time-varying external disturbance; and matrices $\mathbf{A}$ and $\mathbf{B}$ are given by

$$
A = \begin{bmatrix} 0 & 1 & 0 & \cdots & 0 \\ 0 & 0 & 1 & \cdots & 0 \\ \vdots & \vdots & \vdots & \ddots & \vdots \\ 0 & 0 & 0 & \cdots & 1 \\ 0 & 0 & 0 & \cdots & 0 \end{bmatrix}_{n \times n}, \quad B = \begin{bmatrix} 0 \\ 0 \\ \vdots \\ 0 \\ 1 \end{bmatrix}_{n \times 1}
$$

The perturbation of system (6) is defined as Q. Wu (2002, 2004); J. Chen (2014); B. Yang (2015)

$$
\Psi(\cdot) = a(x) + (b(x) - b_0)u + \xi(t) \tag{7}
$$

where b_0 is the constant control gain.

Define a fictitious state to represent the perturbation, i.e., $x_{n+1} = \Psi(\cdot)$. The original nth-order system (6) can be extended into the $(n+1)$th-order system as follows

$$
\dot{x}_{\mathrm{e}} = A_0 x_{\mathrm{e}} + B_1 u + B_2 \dot{\Psi}(\cdot) \tag{8}
$$

where $\quad \mathbf{x}_{\mathrm{e}} = [x_1, x_2, \cdots, x_n, x_{n+1}]^{\mathrm{T}}. \quad \mathbf{B}_1 = [0, 0, \ldots, b_0, 0]^{\mathrm{T}} \in \mathbb{R}^{n+1} \quad$ and $\mathbf{B}_2 = [0, 0, \ldots, 1]^{\mathrm{T}} \in \mathbb{R}^{n+1}$. Matrix $\mathbf{A}_0$ is

$$
A_0 = \begin{bmatrix} 0 & 1 & \cdots & \cdots & 0 \\ 0 & 0 & 1 & \cdots & 0 \\ \vdots & \vdots & \vdots & \ddots & \vdots \\ 0 & 0 & 0 & \cdots & 1 \\ 0 & 0 & 0 & \cdots & 0 \end{bmatrix}_{(n+1) \times (n+1)}
$$

Throughout this paper, $\tilde{x} = x - \hat{x}$ refers to the estimation error of x whereas $\hat{x}$ represents the estimate of x. The following assumptions are made Q. Wu (2004); J. Chen (2014); B. Yang (2015); K. Youcef (1992)

- A.1 b_0 is chosen to satisfy: $|b(x)/b_0 - 1| \le \theta < 1$, where θ is a positive constant.
- A.2 The functions $\Psi(x, u, t) : \mathbb{R}^n \times \mathbb{R} \times \mathbb{R}^+ \mapsto \mathbb{R}$ and $\dot{\Psi}(x, u, t) : \mathbb{R}^n \times \mathbb{R} \times \mathbb{R}^+ \mapsto \mathbb{R}$ are locally Lipschitz in their arguments and bounded over the domain of interest, with $\Psi(0, 0, 0) = 0$ and $\dot{\Psi}(0, 0, 0) = 0$.

Under the above two assumptions, a $(n + 1)$th-order HGSPO is used to estimate $\hat{x}_{\mathrm{e}}$ for system (8) as

$$\dot{\hat{x}}_{\mathrm{e}} = A_0 \hat{x}_{\mathrm{e}} + B_1 u + H(x_1 - \hat{x}_1) \tag{9}$$

where $\mathbf{H} = [\alpha_1/\epsilon, \alpha_2/\epsilon^2, \cdots, \alpha_n/\epsilon^n, \alpha_{n+1}/\epsilon^{n+1}]^{\mathrm{T}}$ is the observer gain. $\alpha_i = C_{n+1}^i \lambda^i$, $i = 1, 2, \cdots, n + 1$, places the observer pole at $-\lambda$, where $\lambda > 0$ and $0 < \epsilon \ll 1$.

Remark 1. This paper adopts the HGSPO Q. Wu (2004); J. Chen (2014); B. Yang (2015) due to its merits of easy analysis of the closed-loop system stability compared to that of sliding-mode perturbation estimator S. Kwon (2004) and nonlinear observer based ADRC J. Han (2009). They are all based on ESO and can provide almost the same performance of perturbation estimation. Note that the implementation feasibility of HGSPO has been verified via hardware-in-the-loop (HIL) test by author in B. Yang (2015).

Using the estimate of states and perturbation, the POAPC for system (6) is designed as

$$\begin{cases} u = b_0^{-1} \left(-\hat{\Psi}(\cdot) - K\hat{x} + \nu \right) \\ \nu = -\phi(y) \end{cases} \tag{10}$$

where ν is an additional input; $\phi(y)$ is any smooth function satisfying $\phi(0) = 0$ and $y\phi(y) > 0$ for all $y \ne 0$; $\mathbf{K} = [k_1, k_2, \cdots, k_n]$ is the feedback control gain, which makes matrix $\mathbf{A}_1 = \mathbf{A} - \mathbf{BK}$ Hurwitzian.

The design procedure of POAPC for system (6) can be summarized as follows:

Step 1: Define perturbation (7) for the original nth-order system (6);

Step 2: Define a fictitious state $x_{n+1} = \Psi(\cdot)$ to represent perturbation (7);

Step 3: Extend the original nth-order system (6) into the extended $(n + 1)$th-order system (8);

Step 4: Design the $(n + 1)$th-order HGSPO (9) for the extended $(n + 1)$th-order system (8) to obtain the state estimate $\hat{x}$ and the perturbation estimate $\hat{\Psi}(\cdot)$ by only the measurement of x_1;

Step 5: Design controller (10) for the original nth-order system (6).

POAPC Design for the VSC-MTDC System

Rectifier controller design

Denote the jth VSC as the rectifier such that DC voltage $V_{\mathrm{dc}j}$ and reactive power Q_j can be regulated to their references $V_{\mathrm{dc}j}^*$ and Q_j^*, respectively. Define the tracking error $\mathbf{e}_j = [e_{j1}, e_{j2}]^{\mathrm{T}} = [V_{\mathrm{dc}j} - V_{\mathrm{dc}j}^*, Q_j - Q_j^*]^{\mathrm{T}}$, differentiate $\mathbf{e}_j$ until control inputs $u_{\mathrm{q}j}$ and $u_{\mathrm{d}j}$ appear explicitly, gives

$$
\begin{cases}
\ddot{e}_{j1} &= \frac{3V_{\mathrm{sq}j}}{2C_j V_{\mathrm{dc}j}}\left[-\frac{R_j}{L_j}I_{\mathrm{q}j} + \omega_j I_{\mathrm{d}j} - \frac{I_{\mathrm{q}j}}{C_j V_{\mathrm{dc}j}}\left(\frac{3V_{\mathrm{sq}j}I_{\mathrm{q}j}}{2V_{\mathrm{dc}j}} - I_{\mathrm{c}j} \right) \right] \\
& \quad -\frac{1}{C_j L_{\mathrm{c}j}}(V_{\mathrm{dc}j} - R_{\mathrm{c}j}I_{\mathrm{c}j} - V_{\mathrm{cc}}) + \frac{3V_{\mathrm{sq}j}}{2C_j L_j V_{\mathrm{dc}j}}u_{\mathrm{q}j} - \ddot{V}_{\mathrm{dc}j}^* \\
\dot{e}_{j2} &= \frac{3V_{\mathrm{sq}j}}{2}\left(-\frac{R_j}{L_j}I_{\mathrm{d}j} + \omega_j I_{\mathrm{q}j} + \frac{V_{\mathrm{sq}j}}{L_j} \right) + \frac{3V_{\mathrm{sq}j}}{2L_j}u_{\mathrm{d}j} - \dot{Q}_j^*
\end{cases}
\tag{11}
$$

It can be seen that system (11) includes two decoupled SISO subsystems, in which $V_{\mathrm{dc}j}$ is controlled by $u_{\mathrm{q}j}$ and Q_j is controlled by $u_{\mathrm{d}j}$, respectively.

The perturbations of system (11) are defined as

$$
\Psi_{j1}(\cdot) = \frac{3V_{\mathrm{sq}j}}{2C_j V_{\mathrm{dc}j}}\left[-\frac{R_j}{L_j}I_{\mathrm{q}j} + \omega_j I_{\mathrm{d}j} - \frac{I_{\mathrm{q}j}}{C_j V_{\mathrm{dc}j}}\left(\frac{3V_{\mathrm{sq}j}I_{\mathrm{q}j}}{2V_{\mathrm{dc}j}} - I_{\mathrm{c}j} \right) \right]
$$

$$
\quad -\frac{1}{C_j L_{\mathrm{c}j}}(V_{\mathrm{dc}j} - R_{\mathrm{c}j}I_{\mathrm{c}j} - V_{\mathrm{cc}}) + (\frac{3V_{\mathrm{sq}j}}{2C_j L_j V_{\mathrm{dc}j}} - b_{j1})u_{\mathrm{q}j}
$$

$$
\Psi_{j2}(\cdot) = \frac{3V_{\mathrm{sq}j}}{2}\left(-\frac{R_j}{L_j}I_{\mathrm{d}j} + \omega_j I_{\mathrm{q}j} + \frac{V_{\mathrm{sq}j}}{L_j} \right) + (\frac{3V_{\mathrm{sq}j}}{2L_j} - b_{j2})u_{\mathrm{d}j}
$$

And system (11) can be expressed by

$$
\begin{cases}
\ddot{e}_{j1} = \Psi_{j1}(\cdot) + b_{j1}u_{\mathrm{q}j} - \ddot{V}_{\mathrm{dc}j}^* \\
\dot{e}_{j2} = \Psi_{j2}(\cdot) + b_{j2}u_{\mathrm{d}j} - \dot{Q}_j^*
\end{cases}
\tag{12}
$$

where b_{j1} and b_{j2} are constant control gains.

A third-order HGSPO is designed to estimate $\Psi_{j1}(\cdot)$ as

$$
\begin{cases}
\dot{\hat{V}}_{\mathrm{dc}j} = \frac{\alpha_{j1}}{\epsilon}(V_{\mathrm{dc}j} - \hat{V}_{\mathrm{dc}j}) + \dot{\hat{V}}_{\mathrm{dc}j} \\
\dot{\hat{\dot{V}}}_{\mathrm{dc}j} = \hat{\Psi}_{j1}(\cdot) + \frac{\alpha_{j2}}{\epsilon^2}(V_{\mathrm{dc}j} - \hat{V}_{\mathrm{dc}j}) + b_{j1}u_{\mathrm{q}j} \\
\dot{\hat{\Psi}}_{j1}(\cdot) = \frac{\alpha_{j3}}{\epsilon^3}(V_{\mathrm{dc}j} - \hat{V}_{\mathrm{dc}j})
\end{cases}
\tag{13}
$$

Then a second-order high-gain perturbation observer (HGPO) is designed to estimate $\Psi_{j2}(\cdot)$ as

$$
\begin{cases}
\dot{\hat{Q}}_j = \hat{\Psi}_{j2}(\cdot) + \frac{\alpha_{j1}'}{\epsilon}(Q_j - \hat{Q}_j) + b_{j2}u_{\mathrm{d}j} \\
\dot{\hat{\Psi}}_{j2}(\cdot) = \frac{\alpha_{j2}'}{\epsilon^2}(Q_j - \hat{Q}_j)
\end{cases}
\tag{14}
$$

where $\alpha_{j1}, \alpha_{j2}, \alpha_{j3}, \alpha_{j1}'$, and α_{j2}' are observer gains, with $0 < \epsilon \ll 1$.

The POAPC for system (11) using the estimate of states and perturbations is designed as

$$
\begin{cases}
u_{qj} = b_{j1}^{-1}[-\hat{\Psi}_{j1}(\cdot) - k_{j1}(\hat{V}_{dcj} - V_{dcj}^*) - k_{j2}(\hat{\dot{V}}_{dcj} - \dot{V}_{dcj}^*) + \ddot{V}_{dcj}^* + \nu_{j1}] \\
u_{dj} = b_{j2}^{-1}(-\hat{\Psi}_{j2}(\cdot) - k_{j1}'(\hat{Q}_j - Q_j^*) + \dot{Q}_j^* + \nu_{j2})
\end{cases}
$$

(15)

where k_{j1}, k_{j2} and k_{j1}' are feedback control gains and $\mathbf{V}_j = [\nu_{j1}, \nu_{j2}]^{\mathrm{T}}$ is an additional system input.

Choose the output of system (11) as $\mathbf{Y}_j = [Y_{j1}, Y_{j2}]^{\mathrm{T}} = [\dot{V}_{dcj} - \dot{V}_{dcj}^*, Q_j - Q_j^*]^{\mathrm{T}}$. Then let $\mathbf{V}_j = [-\lambda_{j1}Y_{j1}, -\lambda_{j2}Y_{j2}]^{\mathrm{T}}$, where λ_{j1} and λ_{j2} are some positive constants to inject an extra system damping into system (11). Based on the passivity theory, the closed-loop system is output strictly passive from output $\mathbf{Y}_j$ to input $\mathbf{V}_j$ B. Yang (2015).

Constants b_{j1} and b_{j2} must satisfy following inequalities to guarantee the convergence of estimation error when the VSC operates within its normal region:

$$
3V_{sqj}/[2C_j L_j V_{dcj}(1-\theta_{j1})] \geq b_{j1} \geq 3V_{sqj}/[2C_j L_j V_{dcj}(1+\theta_{j1})]
$$
$$
3V_{sqj}/[2L_j(1-\theta_{j2})] \geq b_{j2} \geq 3V_{sqj}/[2L_j(1+\theta_{j2})]
$$

where $0 < \theta_{j1} < 1$ and $0 < \theta_{j2} < 1$.

During the most severe disturbance, both DC voltage and reactive power reduce from their initial values to around zero within a short period of time Δ. Thus the boundary values of the estimate of states and perturbations are limited as $|\hat{V}_{dcj}| \leq |V_{dcj}^*|$, $|\hat{\dot{V}}_{dcj}| \leq |V_{dcj}^*|/\Delta$, $|\hat{\Psi}_{j1}(\cdot)| \leq |V_{dcj}^*|/\Delta^2$, $|\hat{Q}_j| \leq |Q_j^*|$, and $|\hat{\Psi}_{j2}(\cdot)| \leq |Q_j^*|/\Delta$, respectively.

The structure of rectifier controller is illustrated by Fig. 3, in which only the measurement of DC voltage V_{dcj} and reactive power Q_j is needed for the controller and observer design.

Inverter controller design

The kth VSC is chosen as the inverter to regulate active power P_k and reactive power Q_k to their references P_k^* and Q_k^*, respectively, where $k = 1, \cdots, N$ and $k \neq j$. Define tracking error $\mathbf{e}_k = [e_{k1}, e_{k2}]^{\mathrm{T}} = [P_k - P_k^*, Q_k - Q_k^*]^{\mathrm{T}}$, differentiate $\mathbf{e}_k$ until control inputs u_{qk} and u_{dk} appear explicitly, gives

$$
\begin{cases}
\dot{e}_{k1} = \frac{3V_{sqk}}{2}\left(-\frac{R_k}{L_k}I_{qk} - \omega_k I_{dk}\right) + \frac{3V_{sqk}}{2L_k}u_{qk} - \dot{P}_k^* \\
\dot{e}_{k2} = \frac{3V_{sqk}}{2}\left(-\frac{R_k}{L_k}I_{dk} + \omega_k I_{qk} + \frac{V_{sqk}}{L_k}\right) + \frac{3V_{sqk}}{2L_k}u_{dk} - \dot{Q}_k^*
\end{cases}
$$

(16)

It can be seen that system (16) includes two decoupled SISO subsystems, in which P_k is controlled by u_{qk} and Q_k is controlled by u_{dk}, respectively.

The perturbations of system (16) are defined as

$$
\Psi_{k1}(\cdot) = \frac{3V_{sqk}}{2}\left(-\frac{R_k}{L_k}I_{qk} - \omega_k I_{dk}\right) + (\frac{3V_{sqk}}{2L_k} - b_{k1})u_{qk}
$$

$$
\Psi_{k2}(\cdot) = \frac{3V_{sqk}}{2}\left(-\frac{R_k}{L_k}I_{dk} + \omega_k I_{qk} + \frac{V_{sqk}}{L_k}\right) + (\frac{3V_{sqk}}{2L_k} - b_{k2})u_{dk}
$$
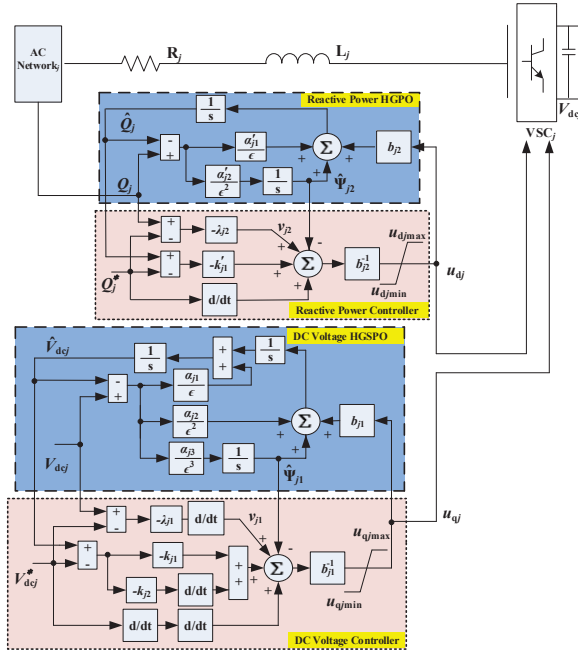
Figure 3. Structure of the rectifier controller.

And system (16) can be expressed by

$$\begin{cases} \dot{e}_{k1} = \Psi_{k1}(\cdot) + b_{k1}u_{\mathrm{q}k} - \dot{P}_k^* \\ \dot{e}_{k2} = \Psi_{k2}(\cdot) + b_{k2}u_{\mathrm{d}k} - \dot{Q}_k^* \end{cases} \tag{17}$$

where b_{k1} and b_{k2} are constant control gains.

A second-order HGPO is designed to estimate $\Psi_{k1}(\cdot)$ as

$$\begin{cases} \dot{\hat{P}}_k = \hat{\Psi}_{k1}(\cdot) + \frac{\alpha_{k1}}{\epsilon}(P_k - \hat{P}_k) + b_{k1}u_{\mathrm{q}k} \\ \dot{\hat{\Psi}}_{k1}(\cdot) = \frac{\alpha_{k2}}{\epsilon^2}(P_k - \hat{P}_k) \end{cases} \tag{18}$$

Similarly, a second-order HGPO is designed to estimate $\Psi_{k2}(\cdot)$ as

$$\begin{cases} \dot{\hat{Q}}_k = \hat{\Psi}_{k2}(\cdot) + \frac{\alpha'_{k1}}{\epsilon}(Q_k - \hat{Q}_k) + b_{k2}u_{\mathrm{d}k} \\ \dot{\hat{\Psi}}_{k2}(\cdot) = \frac{\alpha'_{k2}}{\epsilon^2}(Q_k - \hat{Q}_k) \end{cases} \tag{19}$$

where α_{k1}, α_{k2}, α'_{k1}, and α'_{k2} are observer gains.

The POAPC for system (16) using the estimate of states and perturbations is designed as

$$\begin{cases} u_{\mathrm{q}k} = b_{k1}^{-1}(-\hat{\Psi}_{k1}(\cdot) - k_{k1}(\hat{P}_k - P_k^*) + \dot{P}_k^* + \nu_{k1}) \\ u_{\mathrm{d}k} = b_{k2}^{-1}(-\hat{\Psi}_{k2}(\cdot) - k'_{k1}(\hat{Q}_k - Q_k^*) + \dot{Q}_k^* + \nu_{k2}) \end{cases} \tag{20}$$
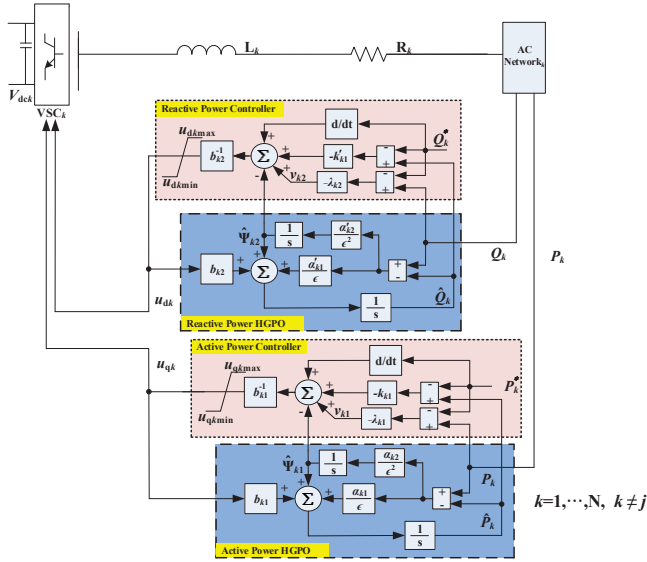
Figure 4. Structure of the inverter controller.

where k_{k1} and k'_{k1} are feedback control gains and $\mathbf{V}_k = [\nu_{k1}, \nu_{k2}]^{\mathrm{T}}$ is an additional system input.

Choose the output of system (16) as $\mathbf{Y}_k = [Y_{k1}, Y_{k2}]^{\mathrm{T}} = [P_k - P_k^*, Q_k - Q_k^*]^{\mathrm{T}}$. Let $\mathbf{V}_k = [-\lambda_{k1}Y_{k1}, -\lambda_{k2}Y_{k2}]^{\mathrm{T}}$, where λ_{k1} and λ_{k2} are some positive constants to inject an extra system damping into system (16). And the closed-loop system is output strictly passive from output $\mathbf{Y}_k$ to input $\mathbf{V}_k$.

Similarly, constants b_{k1} and b_{k2} must satisfy:

$$3V_{\mathrm{sq}k}/[2L_k(1 - \theta_{k1})] \geq b_{k1} \geq 3V_{\mathrm{sq}k}/[2L_k(1 + \theta_{k1})]$$
$$3V_{\mathrm{sq}k}/[2L_k(1 - \theta_{k2})] \geq b_{k2} \geq 3V_{\mathrm{sq}k}/[2L_k(1 + \theta_{k2})]$$

where $0 < \theta_{k1} < 1$ and $0 < \theta_{k2} < 1$.

Again, the boundary values of the estimate of states and perturbations are limited by $|\hat{P}_k| \leq |P_k^*|$, $|\hat{\Psi}_{k1}(\cdot)| \leq |P_k^*|/\Delta$, $|\hat{Q}_k| \leq |Q_k^*|$, and $|\hat{\Psi}_{k2}(\cdot)| \leq |Q_k^*|/\Delta$, respectively.

The structure of inverter controller is illustrated by Fig. 4, in which only the measurement of active power P_k and reactive power Q_k is needed for the controller and observer design. Note that the references of active power, reactive power, and DC voltage are given by the power system operators to satisfy the transmission of electrical power or maintain power system stability through VSC-MTDC systems, which derivative is calculated by directly differentiating the references.

Remark 2. Notice a derivative-control term $\dot{V}_{\mathrm{dc}j}$ is used in the additional input v_{j1}, one effective way to reduce the malignant effect of using such derivative-control term is by
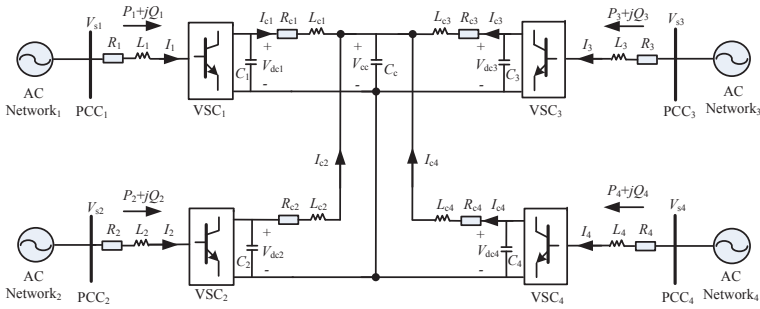
Figure 5. A four-terminal VSC-MTDC system.

Table 1. System parameters used in the four-terminal VSC-MTDC system.

Base power	S_{base}=100 MVA
AC base voltage	V_{ACbase}=132 kV
DC base voltage	V_{DCbase}=150 kV
AC system resistance (25 km)	$R_1 = R_2 = R_3 = R_4 = 0.05\ \Omega/\text{km}$
AC system inductance (25 km)	$L_1 = L_2 = L_3 = L_4 = 0.026\ \text{mH/km}$
DC cable resistance (50 km)	$R_{\text{c1}} = R_{\text{c2}} = R_{\text{c3}} = R_{\text{c4}} = 0.01\ \Omega/\text{km}$
DC cable inductance (50 km)	$L_{\text{c1}} = L_{\text{c2}} = L_{\text{c3}} = L_{\text{c4}} = 0.076\ \text{mH/km}$
DC link capacitance	$C_1 = C_2 = C_3 = C_4 = 7.96\ \mu\text{F}$
Common DC capacitance	$C_C = 19.95\ \mu\text{F}$

Table 2. Control parameters used in the four-terminal VSC-MTDC system.

	Rectifier controller parameters		
Controller	$k_{11} = 100$	$k_{12} = 20$	$\lambda_{11} = 5$
	$b_{11} = 2$	$k'_{11} = 70$	$\lambda_{12} = 5$
	$b_{12} = 0.05$		
Observer	$\alpha_{11} = 1200$	$\alpha_{12} = 4.8 \times 10^5$	$\alpha_{13} = 6.4 \times 10^7$
	$\alpha'_{11} = 400$	$\alpha'_{12} = 4 \times 10^4$	$\Delta = 0.05\ s$
	$\epsilon = 0.1$		
	Inverter controller parameters, $k = 2, 3, 4$		
Controller	$k_{\text{k1}} = 70$	$k'_{\text{k1}} = 70$	$b_{\text{k1}} = 0.1$
	$b_{\text{k2}} = 0.1$	$\lambda_{\text{k1}} = 5$	$\lambda_{\text{k2}} = 5$
Observer	$\alpha_{\text{k1}} = 400$	$\alpha_{\text{k2}} = 4 \times 10^4$	$\alpha'_{\text{k1}} = 400$
	$\alpha'_{\text{k2}} = 4 \times 10^4$	$\Delta = 0.05\ s$	$\epsilon = 0.1$

the introduction of a low-pass filter for DC voltage $V_{\text{dc}j}$, such that the negative effect of measurement noises and the errors amplified through the differentiation can be reduced.

Case Studies

The proposed approach is applied on a four-terminal VSC-MTDC system illustrated by Fig. 5, the system parameters are taken from the two-terminal VSC-HVDC system used by A. Moharana (2010) and extended into four-terminal VSC-MTDC system, in which VSC_1 is chosen as the rectifier to regulate DC voltage and reactive power, while the other three VSCs are chosen as inverters to independently control the active and reactive power.
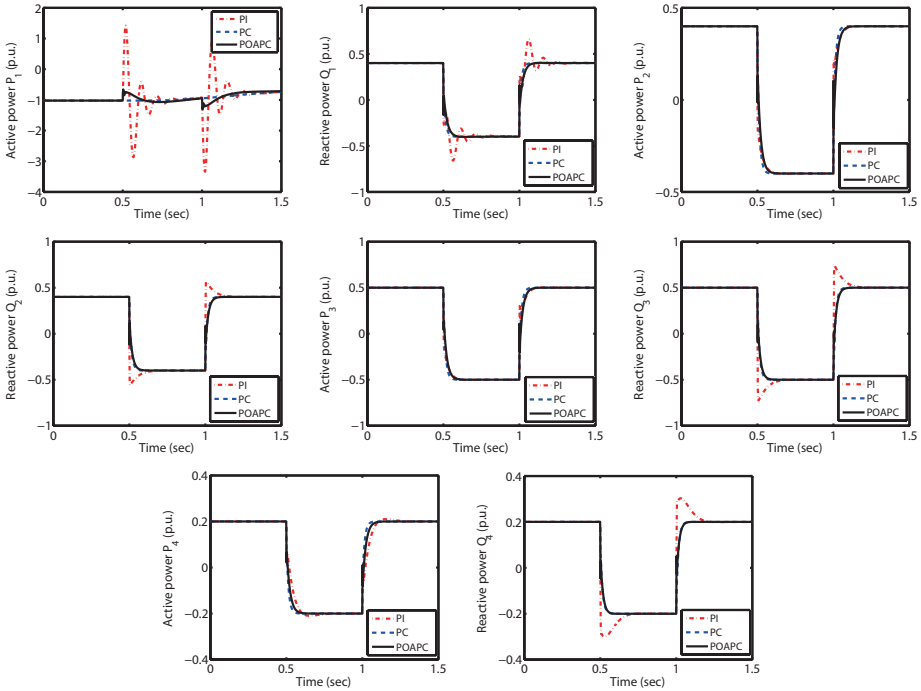
Figure 6. System responses obtained in active and reactive power reversals.

The system frequency of AC network$_4$ is 60 Hz, while the others are 50 Hz. The four-terminal VSC-MTDC system parameters and the control parameters of POAPC are given in Table 1 and Table 2, respectively. The control performance of POAPC is evaluated under various operating conditions in a wide neighbourhood of initial operating points, and compared to that of PI control S. Li (2010) and PC. The control inputs are bounded as $|u_{q1}| \leq 0.8$ per unit (p.u.), $|u_{d1}| \leq 0.6$ p.u., $|u_{qk}| \leq 0.8$ p.u., and $|u_{dk}| \leq 0.6$ p.u. due to the security requirement of converters, such that the overall control inputs satisfy $\sqrt{u_{q1}^2 + u_{q2}^2} \leq 1.0$ p.u. and $\sqrt{u_{qk}^2 + u_{qk}^2} \leq 1.0$ p.u.D. Jovcic (2015).

1) Case 1: Active and reactive power reversals. An active and reactive power reversal started at $t = 0.5$ s and restored to the original value at $t = 1$ s has been tested, while DC voltage is regulated at the rated value $V_{dc1}^* = 1.0$ p.u.. Note that power reversal is a main objective of VSC-MTDC systems which requires the references to be step-like functions to achieve a fast power changing, this can be easily realized as VSC-MTDC systems use the power electronics which can respond and operate very rapidly S. Ruan (2007); S. Li (2010). The system responses are illustrated by Fig. 6. One can find POAPC is able to achieve as satisfactory tracking performance as that of PC, the tiny difference is due to the estimation error. Note that the tracking performance of active power P_1 of POAPC is not very satisfactory compared to that of PC, this is due to the accumulated
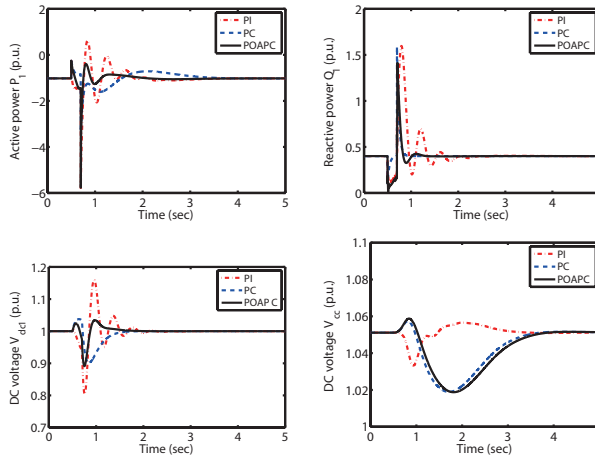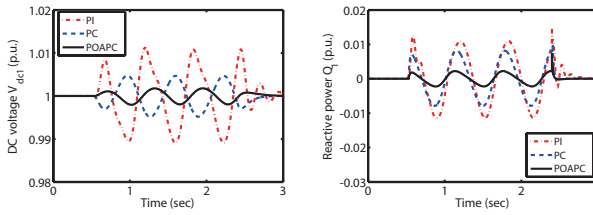
Figure 7. System responses obtained under a 10-cycle LLLG fault at bus 1.

estimation error of P_2, P_3, and P_4, as P_1 is not directly controlled but obtained through the power balance of P_2, P_3, and P_4. Furthermore, POAPC and PC can maintain a consistent control performance and reduce the overshoot of active and reactive power through the perturbation compensation, while PI control cannot maintain a consistent control performance under varied operating points as its control parameters are based on the local system linearization.

2) Case 2: 10-cycle line-line-line-ground (LLLG) fault at AC bus 1. A 10-cycle LLLG fault occurs at bus 1 from 0.5 s to 0.7 s. Due to the fault, the AC voltage at bus 1 is decreased to a critical level. Fig. 7 shows that POAPC and PC can effectively restore the system with less active power oscillations than that of PI control. Due to the large drop of AC voltage, instantaneous demand of reactive power Q_1 increases and a spike of active and reactive power appears expectedly, which is due to the peaking phenomenon of the large observer gains used in the POAPC. To reduce the spike, the observer gains of POAPC need to be reduced but the perturbation estimation rate will be decelerated, thus a compromise between the reduction of the spike magnitude and perturbation estimation rate must be made.

3) Case 3: Offshore wind farm connection. In order to investigate the effect of the penetration of renewable energy into the VSC-MTDC system, AC network$_1$ is connected to an offshore wind farm. Under such framework, the offshore wind farm becomes a weak power grid which voltage is no longer a constant. A voltage change occurs from 0.5 s to 2.5 s caused by the wind speed variation is simulated, in which a time-varying $V_{s1} = 1 + 0.15 \sin(0.2\pi t)$ is assumed. System responses are illustrated in Fig. 8, which shows that POAPC can effectively regulate the active and reactive power as its design does not need an accurate system model.

4) Case 4: Uncertainties in the system resistance and inductance. When there is a fault in the transmission or distribution grid, the resistance and inductance values of the grid

Figure 8. System responses obtained when an offshore wind farm is connected to the VSC-MTDC system.
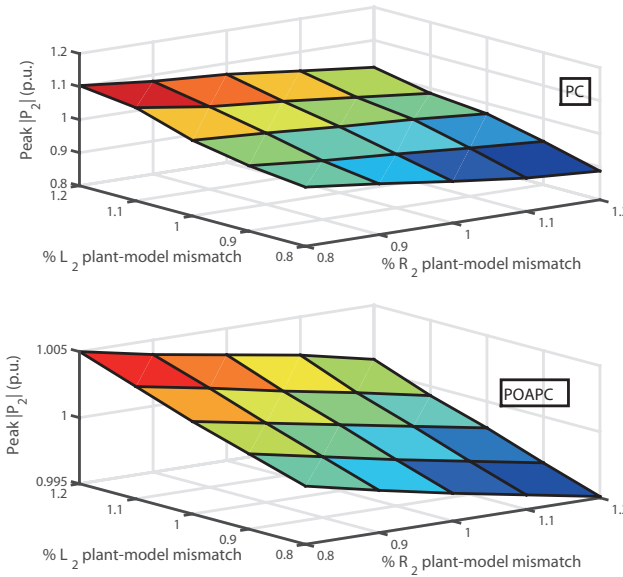
Figure 9. The peak active power $|P_2|$ (in p.u.) to a 30% grid voltage V_{s2} drop for plant-model mismatches in the range of 20% (different parameters may change at the same time).

may change significantly. Several simulations are performed for plant-model mismatches of R_2 and L_2 at the same time with $\pm 20\%$ uncertainties. All tests are undertaken under the nominal grid voltage and a corresponding 30% grid voltage V_{s2} drop at 0.1 s. From Fig. 9 one can find the magnitude of changes is around 10% under the PC and almost does not change under the POAPC. This is because the POAPC can rapidly estimate and compensate all parameter uncertainties, thus a greater robustness can be provided by POAPC than that of PC which requires the accurate system parameters.

The integral of absolute error (IAE) indices of each approach calculated in different cases are tabulated in Table 3. Here $\text{IAE}_x = \int_0^T |x - x^*| \mathrm{d}t$ and x^* is the reference value of variable x. The simulation time T=5 s. Note that POAPC has a little bit higher

IAE than that of PC in the power reversal due to the estimation error, while it can provide much better robustness in the case of 10-cycle LLLG fault and offshore windfarm connection as it does not require an accurate system model. In particular, its IAE_{Q_1} and $\text{IAE}_{V_{dc1}}$ are only 31.92% and 26.43% of those of PI control, 39.75% and 38.76% of those of PC with the offshore windfarm connection. Finally, the overall control efforts of different approaches are presented in Fig. 10, here $\text{IAE}_u = \int_0^T \sum_{i=0}^{n=4} (|u_{qi}| + |u_{di}|)dt$, one can find POAPC needs similar control efforts to that of PI control and PC but provides great robustness.

Table 3. IAE indices (in p.u.) of different control schemes calculated in different cases

Method \ Case	Power reversal			
	IAE_{P_1}	IAE_{Q_1}	IAE_{P_2}	IAE_{Q_2}
PI	7.83E-01	3.19E-02	8.23E-03	1.95E-02
PC	2.19E-02	5.73E-03	6.29E-03	4.88E-03
POAPC	4.33E-02	6.59E-03	6.95E-03	5.34E-03
	IAE_{P_3}	IAE_{Q_3}	IAE_{P_4}	IAE_{Q_4}
PI	7.78E-03	2.64E-02	8.29E-03	4.01E-02
PC	6.01E-03	5.05E-03	6.87E-03	6.15E-03
POAPC	6.76E-03	5.49E-03	7.04E-03	6.43E-03
Method \ Case	10-cycle LLLG fault			
	IAE_{P_1}	IAE_{Q_1}	$\text{IAE}_{V_{dc1}}$	$\text{IAE}_{V_{cc}}$
PI	2.15	1.24	6.28E-01	1.75E-02
PC	1.39	3.37E-01	4.23E-01	8.18E-02
POAPC	0.92	4.12E-01	2.42E-01	8.33E-02
Method \ Case	Offshore wind farm connection			
	IAE_{P_1}	IAE_{Q_1}	$\text{IAE}_{V_{dc1}}$	$\text{IAE}_{V_{cc}}$
PI	6.93E-03	5.89E-03	6.13E-03	5.84E-03
PC	5.19E-03	4.73E-03	4.18E-03	3.96E-03
POAPC	2.33E-03	1.88E-03	1.62E-03	2.13E-03

Conclusion

In this paper, perturbation observer based adaptive passive controllers have been designed for an N-terminal VSC-MTDC system. It only requires the measurement of output variables, i.e. DC voltage, active and reactive power, while no further control parameters tuning is needed once the controller is set.

Case studies have been undertaken on a four-terminal VSC-MTDC system, which verify that the proposed controller can reduce the overshoot of active and reactive power
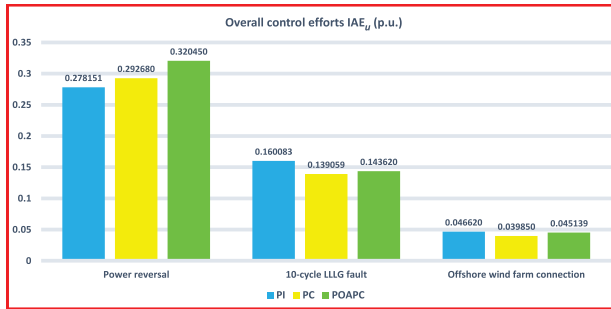
Figure 10. The overall control efforts of different approaches required in each cases.

reversal. In addition, system transient responses have been enhanced under the AC bus fault and offshore wind farm connection as an extra system damping has been injected. Finally, the control performance in the presence of parameter uncertainties has been undertaken, which demonstrates that POAPC can effectively handle the fast time-varying parameter uncertainties and provide a great robustness.

Funding

References

Asplund G (2009) *HVDC grids-possibilities and challenges*, CIGRE SC B4 Bergen Colloq., Bergen, Norway.

Beccuti G, Papafotiou G, and Harnefors L (2014) *Multivariable optimal control of HVDC transmission links with network parameter estimation for weak grids*, IEEE Trans. Control Syst. Technol., vol. 22, no. 2, pp. 676-689.

Bellmunt O, Liang J, Ekanayake J and Jenkins N (2011) *Voltage current characteristics of multiterminal HVDC-VSC for offshore wind farms*, Elect. Power Syst. Res., vol. 81, pp. 440-450.

Bellmunt O, Liang J, King R, Ekanayake J, and Jenkins N (2011) *Topologies of multiterminal HVDC-VSC transmission for large offshore wind farms*, Elect. Power Syst. Res., vol. 81, pp. 271-281.

Chen W, Ballance D, Gawthrop P, and Reilly J (2000) *A nonlinear disturbance observer for robotic manipulators*, IEEE Trans. on Ind. Electron., vol. 47, no. 4, pp. 932-938.

Chaudhuri N and Chaudhuri B (2013) *Adaptive droop control for effective power sharing in multi-terminal DC (MTDC) grids*, IEEE Trans. Power Syst., vol. 28, no. 1, pp. 21-29.

Chen J, Jiang L, Yao W, and Wu Q (2014) *Perturbation estimation based nonlinear adaptive control of a full-rated converter wind turbine for fault ride-through capability enhancement*, IEEE Trans. Power Syst., vol. 29, no. 6, pp. 2733-2743.

Chen W, Yang J, Guo L, and Li S (2016) *Disturbance observer-based control and related methods: An overview*. IEEE Trans. on Ind. Electron., vol. 63, no. 2, pp. 1083-1095.

Flores D, Scherpen J, Liserre M, Vriesand M, Kransse M, and Monopoli V (2014) *Passivity-based control by series/parallel damping of single-phase PWM voltage source converter*, IEEE Trans. Control Syst. Technol., vol. 22, no. 4, pp. 2107-2113.

Flourentzou N, Agelidis G, and Demetriades D (2009) *VSC-based HVDC power transmission systems: an overview*, IEEE Trans. Power Electron., vol. 24, no. 3, pp. 592-602.

Farhang P, Tirtashi M, Noroozian1 R, and Gharehpetian G (2014) *Combined design of VSC-HVDC and PSS controllers for LFO damping enhancement*, Transactions of the Institute of Measurement and Control, vol. 36, no. 4, pp. 529-540.

Gordon S (2006) *Supergrid to the rescue*, Inst. Eng. Technol. Power Eng., vol. 20, pp. 30-33.

Han J (2009). *From PID to active disturbance rejection control*, IEEE Trans. on Ind. Electron., vol. 56, pp. 900-906.

Harnefors L, Yepes A, Vidal A, and Doval J (2015) *Passivity-based controller design of grid-connected VSCs for prevention of electrical resonance instability*, IEEE Trans. Ind. Electron., vol. 62, no. 2, pp. 702-710.

Johnson C(1971) *Accommodation of external disturbances in linear regulator and servomechanism problems*, IEEE Trans. Automat. Contr., vol. 16, no. 6, pp. 635-644.

Jovcic D (2003) *Phase locked loop system for FACTS*, IEEE Trans. Power Syst., vol. 18, no. 3, pp. 1116-1124.

Jovcic D and Ahmed K (2015) *High-voltage direct-current transmission: converters, systems and DC grids*, Wiley-Blackwell, first edition.

Kwon S and Chung W (2004), *Perturbation compensator based robust tracking control and state estimation of mechanical systems*, Springer, New York.

Li S, Haskew T, and Xu L (2010) *Control of HVDC light system using conventional and direct current vector control approaches*, IEEE Trans. Power Electron., vol. 25, no. 12, pp. 3106-3118.

Liang J, Jing T, Bellmunt O, Ekanayake J, and Jenkinsand N (2011) *Operation and control of multiterminal HVDC transmission for offshore wind farms*, IEEE Trans. Power Del., vol. 26, no. 4, pp. 2596-2604.

Li S, Yang J, Chen W, and Chen X. (2014). *Disturbance observer based control: methods and applications*. CRC Press Inc, Taylors and Francis Group.

Meah K and Sadrul Ula A (2008) *Simple fuzzy self-tuning PI controller for multiterminal HVDC transmission systems*, Elect. Power Component and Syst., vol. 36, no. 3, pp. 224-238.

Meah K and Sadrul Ula A (2010) *A new simplified adaptive control scheme for multi-terminal HVDC transmission systems*, Electrical Power and Energy Systems, vol. 32, pp. 243-253.

Moharana A and Dash P (2010) *Input-output linearization and robust sliding-mode controller for the VSC-HVDC transmission link*, IEEE Trans. Power Del., vol. 25, no. 3, pp. 1952-1961.

Preece R and Milanovic J (2014) *Tuning of a damping controller for multiterminal VSC-HVDC grids using the probabilistic collocation method*, IEEE Trans. Power Del., vol. 29, no. 1, pp. 318-326.

Rao H (2015) *Architecture of Nan'ao multi-terminal VSC-HVDC system and its multi-functional control*, CSEE Journal of Power and Energy Systems, vol. 1, no. 1, pp. 9-18.

Ruan S, Li G, Jiao X, Sun Y, and Lie T (2007) *Adaptive control design for VSC-HVDC systems based on backstepping method*, Elect. Power Syst. Res., vol. 77, pp. 559-565.

Tang L and Ooi B (2007) *Locating and isolating DC faults in multiterminal DC systems*, IEEE Trans. Power Del., vol. 22, no. 3, pp. 1877-1884.

Tang Y, He H, and Wen J (2013) *Adaptive control for an HVDC transmission link with FACTS and a wind farm*, Innovative Smart Grid Technologies (ISGT), pp. 1-6.

Wu Q and Jiang L (2002) *Nonlinear adaptive co-ordinated control of multimachine power systems*, Transactions of the Institute of Measurement and Control, vol. 24, no. 3, pp. 195-213.

Wu Q, Jiang L, and Wen J (2004) *Decentralized adaptive control of interconnected non-linear systems using high gain observer*, Int. J. Control, vol. 77, no. 8, pp. 703-712.

Xu L and Yao L (2011) *DC voltage control and power dispatch of a multiterminal HVDC system for integrating large offshore wind farms*, IET Renewable Power Gener., vol. 5, no. 3, pp. 223-233.

Youcef K and Wu S (1992) *Input/output linearization using time delay control*, Journal of Dynamic Systems, Measurement, and Control, vol. 114, no. 1, pp. 10-19.

Yang B, Jiang L, Yao W, and Wu Q (2015) *Perturbation estimation based adaptive coordinated passive control for multimachine power systems*, Control Eng. Pract., vol. 44, pp. 172-192.

Zhong Q and Li K (2004) *Control of uncertain LTI systems based on an uncertainty and disturbance estimator*, Journal of Dynamic Systems, Measurement, and Control, vol. 126, pp. 905-910.

Zhao X and Li K (2015) *Adaptive backstepping droop controller design for multi-terminal high-voltage direct current systems*, IET Gener. Transm. Distrib., vol. 9, no. 10, pp. 975-983.